CHEMISTRY OF MATERIALS

Article

pubs.acs.org/cm

In Situ Synthesis of PbS Nanocrystals in Polymer Thin Films from Lead(II) Xanthate and Dithiocarbamate Complexes: Evidence for Size and Morphology Control

Edward A. Lewis,[†] Paul D. McNaughter,[‡] Zhongjie Yin,[†] Yiqiang Chen,[†] Jack R. Brent,[†] Selina A. Saah,[§] James Raftery,[‡] Johannes A. M. Awudza,[§] M. Azad Malik,[†] Paul O'Brien,*[,†,‡] and Sarah J. Haigh*[,†]

[†]School of Materials and [‡]School of Chemistry, The University of Manchester, Oxford Road, Manchester, M13 9PL, United Kingdom

[§]Department of Chemistry, Kwame Nkrumah University of Science and Technology, Kumasi, Ghana

Supporting Information

ABSTRACT: Lead sulfide has been grown from single molecular precursors within a polymer matrix to form networks of PbS nanocrystals. These materials are model systems for the processing of polymer−nanoparticle layers for flexible hybrid photovoltaic devices. Processing is achieved by spin coating a solution containing the precursor and polymer onto a substrate, followed by heating of the film to decompose the precursor. The effect of precursor chemistry has been explored using lead(II) dithiocarbamates, their 1,10-phen adducts, and lead(II) xanthates with different alkyl chain lengths (butyl, hexyl, and octyl). The xanthates were found to be more promising precursors giving control over nanocrystal size and shape on variation of the alkyl chain length. The lead(II) octyl xanthate complex causes anisotropic growth, forming PbS nanowires within the polymer matrix.

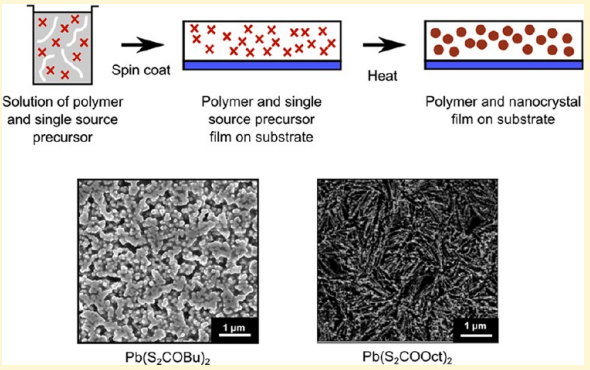

1. INTRODUCTION

Polymer thin films containing inorganic semiconducting nanostructures have been investigated for a wide range of applications including solar cells,[1−5] light emitting diodes,[6−9] photodiodes,[10] and chemical sensors.[11,12] Hybrid photovoltaics combine conjugated polymers with nanoscale inorganic semiconductors and can potentially exploit the properties of both the organic and inorganic components.[13−15] These systems offer potential for band gap engineering,[5] solution processing, and compatibility with roll-to-roll production methods.[13] Nanocomposite polymer films containing inorganic semiconducting nanocrystals are promising materials for next-generation, low cost, lightweight, flexible photovoltaics.[13,16,17]

PbS nanocrystals are considered to be one of the more attractive semiconductor materials for hybrid photovoltaics. Their narrow, size-tunable, band gap facilitates absorption in the near- and mid-infrared regions of the spectrum.[2,18,19] In addition, reports of multiple exciton generation in PbS quantum dots have demonstrated the potential for PbS based devices to exceed the Shockley-Queisser limit.[20−22]

Typically hybrid photovoltaic devices have been fabricated by first synthesizing semiconductor nanocrystals ex situ in the solution phase; long chain ligands are typically employed to control growth and disperse the nanocrystals in organic solvents suitable for film production.[18,23,24] The requirement for ligands that contain long alkyl chains is potentially detrimental to device performance.[14] Insulating ligands prevent charge transfer at polymer−semiconductor interfaces and charge transport through nanocrystal networks.[13,14,25] Attempts to replace long chain ligands with shorter or conducting ligands can improve device performance but add further complexity to the fabrication process.[3,26] Furthermore, such reactions never achieve complete ligand exchange and can reduce colloidal stability, limiting nanocrystal loadings.[14,27]

Many of the difficulties associated with the traditional ex situ synthetic methods can be overcome by employing in situ synthetic routes, where semiconductor nanocrystals are grown within the polymer matrix.[4,5,28−30] In this approach a solution containing both a polymer and a precursor complex is spin coated to form a precursor loaded polymer film. Upon heating decomposition of the precursor occurs causing the growth of inorganic semiconductor nanostructures within the polymer matrix, as illustrated in Figure 1a.[4,5,28,29] This synthetic route involves no additional ligands and consequently allows improved contact at polymer−inorganic interfaces and between adjacent nanocrystals, leading to improved charge separation and transport.[31,32] In situ methods are synthetically simpler and have potential for large scale processing, e.g., roll-to-roll manufacturing.[16,17,30]

Received: December 26, 2014
Revised: February 2, 2015
Published: February 13, 2015

DOI: 10.1021/cm504765z
Chem. Mater. 2015, 27, 2127−2136

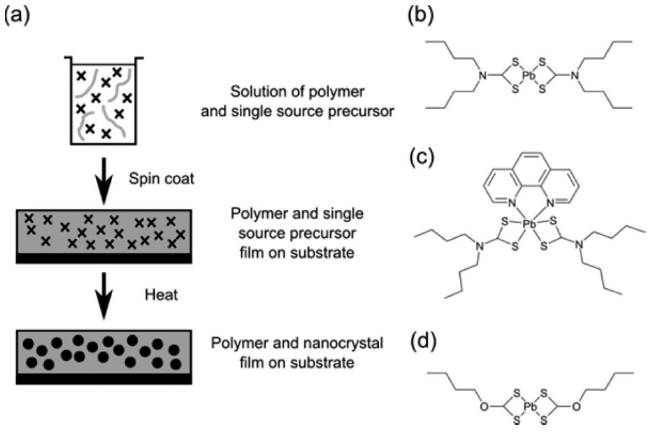

Figure 1. (a) Schematic of the in situ approach employed to fabricate the PbS–polymer films and the precursor families tested: (b) lead(II) dithiocarbamate complexes, (c) a 1,10-phenanthroline adducts of lead(II) dithiocarbamate complexes, and (d) lead(II) xanthate complexes shown with butyl groups.

To date, the only metal sulfides to have been synthesized by the decomposition of single source precursors in a polymer film are CdS,[4,5,32,33] $CuInS_2$,[29] ZnS,[34,35] Bi_2S_3,[36] and Sb_2S_3.[31] Despite an extensive family of single source precursor molecules used for chemical vapor deposition and nanoparticle synthesis,[37−42] relatively few have been investigated within a polymer matrix. Of particular note, metal dithiocarbamate complexes have been widely used as precursors for the synthesis of metal sulfide nanocrystals and thin films but have not been tested with the in situ approach. Considering its attractive properties,[2,20] it is interesting that PbS has not yet been made by an in situ approach.

The lack of size and shape control over nanocrystals synthesized within polymer matrices, to date, is a major disadvantage when compared to ex situ methods. By contrast, precise control over the size and shape of nanocrystals is possible using well established ex situ methods such as hot-injection syntheses.[43−45] It is known that the shape of the nanocrystals used has a huge impact on photovoltaic device performance,[1] e.g., elongated particles improve device performance compared to spheres.[46] Highly attractive nanocrystal architectures are tetrapods and hyperbranched structures.[47]

Optimal photovoltaic cell film morphologies should possess fine phase separation, so excitons are never generated far from an interface, and unhindered pathways should exist for efficient transport of charge carriers to the electrodes.[13,14] To achieve this, highly interconnected nanodimensional networks of nanocrystal and polymer are required.[1,32,46] To fully exploit the potential advantages of the in situ approach it is essential to develop methods for morphological control that are equivalent or superior to those demonstrated for ex situ nanocrystal synthesis.

In this work we investigate the synthesis of PbS–polymer hybrid films using an in situ approach. We focus on exploring new chemistry which could be applicable to PbS containing hybrid photovoltaics. The majority of the existing in situ literature has focused on complexes of ethyl xanthates,[4,5,31,32,48] although a selection of alternate xanthates have been investigated for their potential improved solubility and device performance.[29,33] We explore a broad range of novel precursor chemistry, taking inspiration from the extensive range of xanthate and dithiocarbamate complexes developed for the synthesis of PbS nanocrystals and thin films.[49−52] All precursors investigated are air stable, are soluble in organic solvents, and decompose cleanly to form PbS. We investigate their decomposition in polystyrene, our model polymer matrix. Controlling the morphology of semiconductor–polymer nanocomposites is critical if we are to improve device performance. In this study we focus on understanding how precursor chemistry and heating conditions can be used to control PbS–polymer film morphology.

2. EXPERIMENTAL SECTION

2.1. Chemicals. Potassium ethyl xanthogenate (96%, Sigma-Aldrich), 1-butanol anhydrous (99.8% Sigma-Aldrich), 1-hexanol (reagent grade 98%, Sigma-Aldrich), 1-octanol (anhydrous ≥99%, Sigma-Aldrich), sodium hydride (dry 95%, Sigma-Aldrich), diethylamine (≥99.5%, Sigma-Aldrich), dibutylamine (≥99.5%, Sigma-Aldrich), 1,10-phenanthroline (≥99%, Sigma-Aldrich), ethanol (≥99.8%, Sigma-Aldrich), carbon disulfide (low benzene ≥99.9%, Sigma-Aldrich), lead(II) nitrate (>99%, Fisher Scientific), lead(II) acetate trihydrate (≥99.9%, Sigma-Aldrich), diethyl ether (≥99.8%, Sigma-Aldrich), polystyrene (average molecular weight, M_w ∼280,000 by GPC, Sigma-Aldrich), and potassium hydroxide (>85%, Fisher Scientific) were used, as received, with no further purification.

2.2. Characterization. Elemental analysis and TGA were performed by the University of Manchester Microanalytical Laboratory, using a Thermo Scientific Flash 2000 Organic Elemental Analyzer and a Seiko SSC/S200 model using a heating rate of 10 °C min^{-1} from room temperature to 600 °C in a nitrogen atmosphere. ^{1}H NMR analysis was performed using a Bruker AVANCE III 400 MHz spectrometer.

2.3. Synthesis of Precursors. *Synthesis of Lead(II) Ethylxanthate, $Pb(S_2COEt)_2$ (**1**).* Potassium ethyl xanthogenate (10 g, 62.5 mmol) was dissolved in 750 mL of ethanol and was cooled to 0 °C while stirring. To this a solution of lead(II) nitrate (10.35 g, 31 mmol) dissolved in 100 mL of DI H_2O was added dropwise. The mixture was stirred for a further 30 min. The colorless precipitate which formed was then filtered and washed with DI water and then ethanol. The product was then dried under vacuum overnight. ^{1}H NMR (400 MHz, $CDCl_3$) δ = 4.70 (q, J = 7.1 Hz, 4H; CH_2), 1.52 (t, J = 7.1 Hz, 6H; CH_3). Elemental analysis calcd for $Pb(S_2COEt)_2$: C, 16.04; H, 2.24; S, 28.47. Found: C, 16.24; H, 2.25; S, 28.40. Mp = 145–146 °C.

*Synthesis of Lead(II) n-Butylxanthate, $Pb(S_2COBu)_2$ (**2**).* Potassium hydroxide (2.98 g, 56 mmol) was dissolved in 50 mL of a 1:1 mixture of butanol and DI water while stirring. The solution was cooled to 0 °C, and carbon disulfide (3.5 mL, 58 mmol) was added dropwise. The resulting yellow solution was stirred for an hour before reducing the solvent volume in vacuo. The yellow precipitate, $K(S_2COBu)$, was filtered, washed with a small amount of ice-cold water, and dried under vacuum.

Potassium butylxanthate, $K(S_2COBu)$ (8.0 g, 43 mmol), was dissolved in 100 mL of DI water. Lead(II) nitrate (8.3 g, 25 mmol) was dissolved in 100 mL of DI H_2O and added dropwise to the yellow potassium xanthate solution. A brown precipitate formed which was filtered, washed with DI water and ethanol, and dried under vacuum overnight. Elemental analysis calcd for $Pb(S_2COBu)_2$: C, 23.77; H, 3.59; S, 25.31. Found: C, 23.75; H, 3.79; S, 25.17. ^{1}H NMR (400 MHz, $CDCl_3$) δ = 4.64 (t, J = 6.6 Hz, 4H; CH_2), 1.94–1.80 (m, 4H; CH_2), 1.52–1.37 (m, 4H; CH_2), 0.96 (t, J = 7.4 Hz, 6H; CH_3). Mp = 95–96 °C.

*Synthesis of Lead(II) n-Hexylxanthate, $Pb(S_2COHex)_2$ (**3**).* The synthesis of **3** is the same as **2**, except 1-hexanol was used in place of 1-butanol. A total of 5 g of the crude $Pb(S_2COHex)_2$ was dissolved in dichloromethane (100 mL) and washed three times with DI water. The organic layer was removed and reduced by half under vacuum. Petroleum ether (300 mL) was added to precipitate the product which was isolated by filtration and further washed with a small amount of water and petroleum ether. The product, a light brown powder, was dried under vacuum overnight. Elemental analysis calcd for Pb-

DOI: 10.1021/cm504765z
Chem. Mater. 2015, 27, 2127−2136

$(S_2COHex)_2$: C, 29.95; H, 4.67; S, 22.78. Found: C, 29.90; H, 4.82; S, 22.71. ^{1}H NMR (400 MHz, $CDCl_3$) δ = 4.63 (t, J = 6.7 Hz, 4H; CH_2), 1.97−1.76 (m, 4H, CH_2), 1.48−1.37 (m, 4H; CH_2), 1.37−1.26 (m, 8H), 0.90 (t, J = 7.1 Hz, 6H; CH_3). Mp = 78−79 °C.

*Synthesis of Lead(II) n-Octylxanthate, $Pb(S_2COOct)_2$ (**4**).* Sodium hydride (1.2 g, 50 mmol) and *n*-octanol (7.89 mL, 50 mmol) were combined in 50 mL of diethyl ether and cooled to 0 °C. Carbon disulfide (3.0 mL, 50 mmol) was added dropwise while stirring, and the solution turned yellow. The reaction mixture was allowed to return to room temperature, and lead acetate trihydrate (9.48 g, 25 mmol) dissolved in 50 mL of DI water was added dropwise while stirring, resulting in the formation of a cream precipitate. The precipitate was collected by filtration, washed with DI water, and dried under vacuum. Elemental analysis calcd for $Pb(S_2COHex)_2$: C, 34.99; H, 5.55; S, 20.76. Found: C, 35.01; H, 5.61; S, 20.73. ^{1}H NMR (400 MHz, $CDCl_3$) δ = 4.63 (t, J = 6.7 Hz, 4H; CH_3), 1.94−1.80 (m, 4H; CH_2), 1.47−1.36 (m, 4H; CH_2), 1.36−1.20 (m, 16H), 0.88 (t, J = 6.9 Hz, 6H; CH_3). Mp = 77−78 °C.

*Synthesis of Lead(II) Diethyldithiocarbamate, $Pb(S_2CNEt_2)_2$ (**5**).* Diethylamine (33 mL, 0.32 mol) was diluted in 250 mL of methanol and cooled in an ice bath. Carbon disulfide (19 mL, 0.32 mol) was dissolved in 200 mL of methanol and added to the amine solution dropwise and stirred for 30 min resulting in a yellow solution. A solution of lead(II) acetate trihydrate (61 g, 0.16 mol) in 150 mL of DI water was added dropwise to a stirred solution of the dithiocarbamate resulting in a cream precipitate. The precipitate was collected by filtration and washed with ethanol and then DI water and dried under vacuum. Elemental analysis calcd for $Pb(S_2CNEt_2)_2$: C, 23.86; H, 4.00; N, 5.56. Found C, 24.12; H, 3.97; N, 5.59. ^{1}H NMR (400 MHz, $CDCl_3$) δ = 3.78 (t, J = 7.1 Hz, 8H; CH_2), 1.32 (t, J = 7.1 Hz, 12H; CH_3). Mp = 208−209 °C.

*Synthesis of Lead(II) Dibutyldithiocarbamate, $Pb(S_2CNBu_2)_2$ (**6**).* The synthesis of **6** is the same as **5**, except dibutylamine is used in place of diethylamine. Elemental analysis calcd for $Pb(S_2CNBu_2)_2$: C, 35.12; H, 5.89; N, 4.55. Found: C, 35.07; H, 6.13; N, 4.51. ^{1}H NMR (400 MHz, $CDCl_3$) δ = 3.76−3.61 (m, 8H; CH_2), 1.82−1.66 (m, 8H; CH_2), 1.42−1.27 (m, 8H; CH_2), 0.94 (t, J = 7.4 Hz, 12H; CH_3). Mp = 78−80 °C.

*Synthesis of Lead(II) Diethyldithiocarbamate 1,10-Phenanthroline Adduct, $Pb(S_2CNEt_2)_2$(1,10-phen) (**7**).* **5** (10.1 g, 20 mmol) and 1,10-phenanthroline (4 g, 22 mmol) were dissolved in a mixture of 250 mL of chloroform and 150 mL of toluene. The solution was heated to 40 °C and then held at 40 °C for 20 min. The solvent was removed, leaving a bright yellow solid which was recrystallized from hot toluene. Elemental analysis calcd for $Pb(S_2CNEt_2)_2$(1,10-phen): C, 38.66; H, 4.13; N, 8.19. Found: C, 38.43; H, 4.18; N, 8.06. ^{1}H NMR (400 MHz, $CDCl_3$) δ = 9.20 (dd, J = 4.3, 1.7 Hz, 2H; aryl-H), 8.27 (dd, J = 8.1, 1.8 Hz, 2H; aryl-H), 7.81 (s, 2H; aryl-H), 7.65 (dd, J = 8.1, 4.3 Hz, 2H; aryl-H), 3.78 (q, J = 7.1 Hz, 8H; CH_2), 1.32 (t, J = 7.1 Hz, 12H; CH_3). Mp = 134−137 °C.

*Synthesis of Lead(II) Dibutyldithiocarbamate 1,10-Phenanthroline Adduct, $Pb(S_2CNBu_2)_2$(1,10-phen) (**8**).* The synthesis of **8** is the same as **7**, except that **6** was used in place of **5** and the product was precipitated by dropwise addition of petroleum ether. The precipitate was then filtered, washed with ethanol, and dried under vacuum. Elemental analysis calcd for $Pb(S_2CNBu_2)_2$(1,10-phen): C, 45.26; H, 5.57; N, 7.04. Found: C, 45.27; H, 5.66; N, 7.01. ^{1}H NMR (400 MHz, $CDCl_3$) δ = 9.20 (dd, J = 4.3, 1.7 Hz, 2H; aryl-H), 8.26 (dd, J = 8.1, 1.8 Hz, 2H; aryl-H), 7.81 (s, 2H; aryl-H), 7.65 (dd, J = 8.1, 4.3 Hz, 2H; aryl-H), 3.80−3.55 (m, 8H; CH_2), 1.84−1.65 (m, 8H; CH_2), 1.42−1.22 (m, 8H; CH_2), 0.94 (t, J = 7.4 Hz, 12H; CH_3). Mp = 153−155 °C.

Single crystals of precursor **8** were grown for X-ray crystallography using the vapor diffusion method, using chloroform as the solvent and methanol as the antisolvent. After 1 week large bright yellow crystals were collected.

2.4. Fabrication of Thin Films. Polystyrene (85 mg) and the desired lead complex were dissolved in 2.5 mL of chloroform. The mass of precursor was chosen as necessary to achieve the desired precursor:polymer mass ratio. Initial investigations looked at a range of precursor: polymer ratios. A 6:1 ratio was found to allow the fabrication of high quality films for all precursors and all results presented in this work employ a 6:1 ratio unless stated otherwise. Glass slides were cut to 20 mm × 15 mm to fit the spin coater, cleaned by sonication in acetone, and allowed to dry. A total of 0.2 mL of the precursor−polystryrene solution was coated onto the glass slide by spin coating at 500 rpm for 120 s. The resulting films were allowed to dry and then loaded into a quartz tube for heating. Unless otherwise stated all heating was performed using standard Schlenk techniques under dry nitrogen. The tube was then heated in the tube furnace to the desired temperature at a rate of ∼3 °C s^{-1}. The furnace was held at the chosen temperature for the specified time, and once this time had elapsed the furnace was turned off and the tube allowed to return to room temperature. A schematic showing the key features of the in situ approach can be found in Figure 1a.

2.5. Characterization of Thin Films. X-ray diffraction (XRD) analysis was used to determine the extent of precursor conversion to PbS. Grazing incidence XRD diffraction patterns were acquired using a Bruker D8 Advance diffractometer, using a Cu Kα source with a Göbel mirror optic and Soller slits on the detector side. Scans were acquired at a grazing incidence of 3° over a 2θ range of 15−90° with 0.02° steps and 3 s per step. After XRD analysis, the films were mounted on aluminum stubs with silver paint and carbon coated to reduce charging. Carbon coating was performed using a Gatan precision etching coating system (PECS).

Scanning electron microscope (SEM) imaging was used to determine the morphology of the PbS−polymer hybrid, using an FEI Magellan 400 SEM with a beam current of 0.4 nA, an accelerating voltage of 3 kV, and a concentric backscattered (CBS) detector.

PbS nanostructures were extracted from the PbS−polymer film for higher magnification imaging and size analysis in the transmission electron microscope (TEM). The PbS−polymer films were briefly immersed in chloroform, dissolving the polymer phase and dispersing the PbS nanocrystals. The resulting nanocrystal suspension was drop-cast onto a holey carbon support membrane. The grid was then washed with a drop of clean chloroform to remove any residual polymer. Bright field TEM images and selected area electron diffraction (SAED) patterns were acquired using a Tecnai F30 operated at 300 kV. Particle sizes were determined using ImageJ software.

TEM grids, SEM stubs, and silver paint were all purchased from Agar Scientific UK. Thermo Scientific Menzel Gläzer glass slides were purchased from Fisher Scientific UK.

3. RESULTS AND DISCUSSION

3.1. Precursor Properties. In this work we investigate a range of precursor chemistries to identify single source precursors for the fabrication of hybrid PbS−polymer thin films. An ideal precursor would have a number of properties. First, the precursor should not decompose at ambient temperature or upon exposure to air or moisture. Second, the precursor needs good solubility in organic solvents that also dissolve relevant polymers. Simple solution processing techniques can then be used to prepare films with high precursor loadings. Third, the precursor should decompose at relatively low temperatures as it is vital the heating step does not damage the polymer component of the film. Additionally, interest in flexible solar cells requires compatibility with flexible plastic substrates which are also incompatible with high temperature heating.[17,30,50]

The majority of the literature on in situ fabrication of polymer−metal sulfide photovoltaics has focused on metal ethylxanthate complexes,[4,5,31,32,48] with recent investigations turning to alternative alkyl xanthate complexes.[29,33] However, many variations of metal xanthate complexes and other common single source precursors, such as dithiocarbamate complexes, have not been explored within a polymer matrix.

DOI: 10.1021/cm504765z
Chem. Mater. 2015, 27, 2127−2136

Here, we investigate a number of dithiocarbamate complexes and their 1,10-phenanphroline adducts and compare their performance to xanthates. Complexes that contain longer chained alkyl groups have higher solubility in organic solvents;[29] therefore, we also investigate butyl-, hexyl-, and octyl-xanthate complexes as potential precursors. The structures of the three families of precursors used in this study are shown in Figure 1b–d. Additionally the previously unreported crystal structure of $Pb(S_2CNBu_2)_2$(1,10-phen) is determined (Section 3.2).

Thermogravimetric analysis (TGA) was used to investigate the precursors' thermal decomposition. Supporting Information Figure 1 shows the TGA plots of precursor molecules from each of the three families investigated and our model polymer matrix, polystyrene ($M_W \sim 280\,000$). The onset of thermal decomposition for all the precursors investigated is significantly lower than that of polystyrene. The xanthate family of precursors decompose at significantly lower temperatures (>150 °C lower) than the dithiocarbamate based complexes, while adducting dithiocarbamate complexes with 1,10-phenanphroline produces only a modest decrease in decomposition temperature (Supporting Information Figure 1). It has been suggested that xanthates decompose via the Chugaev elimination, giving only volatile byproducts.[53] For all xanthate complexes the final residual mass is less than one percentage point higher than that calculated for 100% conversion to PbS, suggesting a very clean decomposition.

High precursor solubility in an organic solvent that can also dissolve the polymer component of the hybrid film is vital for high semiconductor loading and compatibility with cheap, high throughput, solution phase processing such as inkjet printing or roll-to-roll techniques.[17,54] In our model system chloroform is used as the film casting solvent. The solubility of the eight precursors is shown in Figure 2. Longer alkyl chains are shown

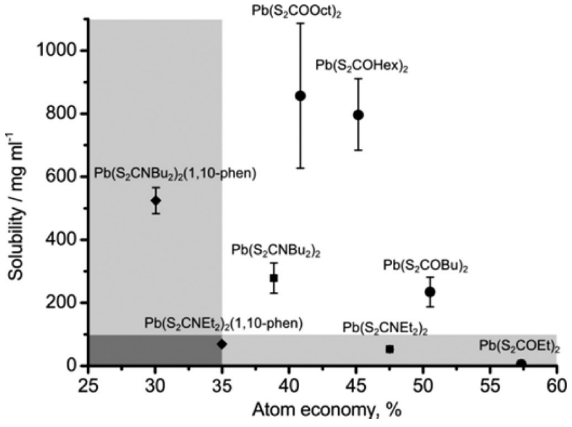

Figure 2. Plot of precursor atom economy against solubility in chloroform with tested xanthate (circles), dithiocarbamates (squares), and 1,10-phen adducted dithiocarbamate (diamonds) complexes shown.

to increase solubility as does addition of the 1,10-phenanthroline ligand to the complex. Dithiocarbamates display higher solubility than xanthates of the same chain length. Another parameter of precursor performance is atom economy, defined as molecular mass of desired product/molecular mass of reactants, while longer chained and/or adducted precursors show improved solubility and are also less atomically efficient. When compared to xanthate complexes of equal chain length, dithiocarbamate complexes show considerably worse atom economy. Figure 2 plots solubility against atom economy; the precursors residing in the top right quadrant are identified as especially attractive due to their combination of high solubility and respectable atom economy. The three long chain xanthate complexes, $Pb(S_2COBu)_2$, $Pb(S_2COHex)_2$, and $Pb(S_2COOct)_2$, stand out as having attractive properties in terms of decomposition temperature, solubility. and atom economy. A table displaying key TGA parameters, solubility, and atom economy for all precursors investigated can be found in the Supporting Information (Table 1).

High precursor loadings are essential for the envisioned applications of these systems. Therefore, the precursors $Pb(S_2CNEt_2)_2$, $Pb(S_2CNEt_2)_2$(1,10-phen), and $Pb(S_2COEt)_2$ were not used further, due to their low solubilities. Our investigations concentrate on the five most promising complexes: $Pb(S_2COBu)_2$, $Pb(S_2COHex)_2$, $Pb(S_2COOct)_2$, $Pb(S_2CNBu_2)_2$, and $Pb(S_2CNBu_2)_2$(1,10-phen).

3.2. Structure of $Pb(S_2CNBu_2)_2$(1,10-phen). The crystal structure of $Pb(S_2CNBu_2)_2$(1,10-phen) is shown in Figure 3

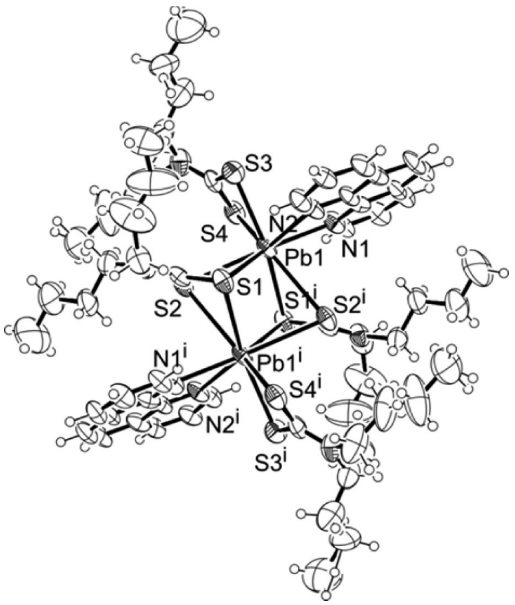

Figure 3. Thermal ellipsoid plot of lead(II) dibutyldithiocarbamate 1,10-phenanthroline adduct, $Pb(S_2CNBu_2)_2$(1,10-Phen), at 50% probability. CCDC reference number 1044935.

with further information in Supporting Information Tables 2 and 3. Unlike the previously reported structure of $Pb(S_2CNEt_2)_2$(1,10-phen), the butyl adduct does not form a dimer with clear dative bonds. Both structures contain a pair of bridging dithiocarbamates with one located *cis* and one *trans* to the adducted phenanthroline. In the ethyl structure the Pb–S bonds that are *trans* to the phenanthroline are 0.3–0.6 Å longer than the *cis* Pb–S bonds. The significant difference in bond lengths between the bridging dithiocarbamate and the metal centers indicates that a dimer with dative interactions between monomers had been formed. In the structure of the butyl adduct this is not seen as the four Pb–S bond lengths of the bridging dithiocarbamates vary by 0.1 Å (Pb(1) to S(1), S(2), $S(1^i)$, and $S(2^i)$ bond lengths in Supporting Information Table 2). In contrast to the ethyl structure, the Pb–S bonds *trans* to the phenanthroline in the butyl structure are slightly shorter than in the *cis* bridging dithiocarbamate. As a consequence the

DOI: 10.1021/cm504765z
Chem. Mater. 2015, 27, 2127–2136

structure is a bimetallic coordination compound and not a dimer with bonding between monomer units.

Primary amines can lower the decomposition temperature of dithiocarbamate complexes,[50,51] and the mechanism has been shown to involve an amine adduct intermediate, with the metal coordinated nitrogen performing nucleophilic attack at the thiocarbonyl carbon.[55] As 1,10-phenanphroline is a poor nucleophile this mechanism is unlikely to be responsible for the lower decomposition temperatures of 1,10-phenanphroline adducts seen here. Comparing the known single crystal structures of $Pb(S_2CNEt_2)_2$(1,10-phen) and $Pb(S_2CNEt_2)_2$[56] shows that the Pb−S bonds are longer in the adducted structure. We believe that the altered coordination around the lead destabilizes the complex.

3.3. Influence of Precursor Structure on Film Morphology. A suitable nanodimensional morphology within hybrid films is critical for good photovoltaic performance. The influence of the precursor structure on the morphological characteristics of films made by the in situ method has yet to be investigated. The effect of precursor chemistry is demonstrated by a comparison of five films prepared with different precursors but under otherwise identical conditions. All films in this work were heated under nitrogen; XRD analysis showed that heating in an inert atmosphere is vital to avoid oxidation. While all films prepared under dry nitrogen show either pure PbS or a mixture of PbS and unreacted precursors, depending upon the time and temperature used, films prepared by heating in air show additional peaks which can be indexed to lead sulfate, $PbSO_4$ (Supporting Information Figure 2).

Upon heating, all precursors yield uniform, adherent, black films (Supporting Information Figure 3). Heating at 275 °C for 30 min results in full decomposition of all precursors to give pure cubic phase PbS (galena) with no unreacted precursor or impurities, e.g., lead sulfates, detected by XRD (Supporting Information Figure 4). The morphology of the PbS−polymer films is found to differ dramatically depending on the precursor used. Backscattered electron (BSE) SEM images of the films reveal dramatic differences in film morphology when using dithiocarbamate (Figure 4a,b) and xanthate (Figure 4c−h) complexes. The dithiocarbamate complexes produce inhomogeneous films containing very large PbS crystal structures, with dimensions ranging from hundreds of nanometers to several micrometers, separated by large regions of polymer containing no PbS. This type of film morphology is unsuitable for photovoltaic applications. By contrast the xanthate complexes ($Pb(S_2COBu)_2$, $Pb(S_2COHex)_2$, and $Pb(S_2COOct)_2$) produce homogeneous film morphologies that are more promising for photovoltaic device applications. All three xanthate derived films contain PbS nanostructures less than 150 nm in size, which are distributed uniformly through the polymer, and show relatively narrow size and shape distributions.

The dramatic change in particle size observed between the dithiocarbamate and xanthate complexes may be explained in terms of precursor reactivity.[57] In the kesterite system (Cu_2ZnSnS_4) the role of precursor reactivity has recently been elucidated.[57] During heating the more reactive precursors decompose rapidly, quickly reaching a supersaturated state and forming a large number of nuclei. In comparison, when a less reactive precursor is used supersaturation is reached more slowly and fewer nuclei form. In both cases, the initial nucleation burst is followed by a period of growth of the existing nuclei until the supply of precursor is exhausted. The final size of particles will be smaller if more nuclei were formed

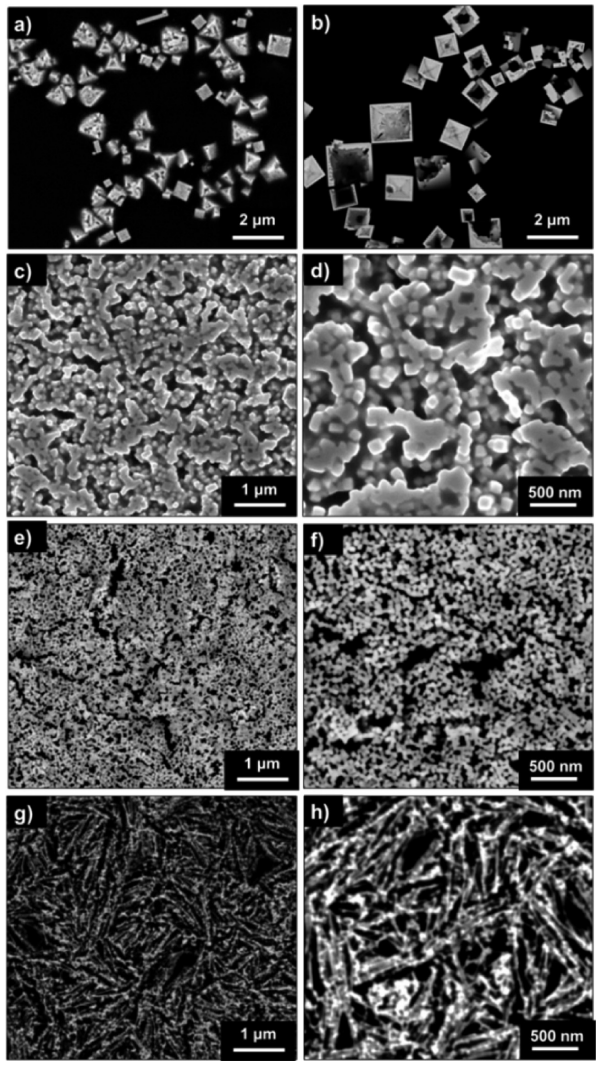

Figure 4. SEM BSE images of films made at 275 °C for 30 min: (a) $Pb(S_2CNBu_2)_2$, (b) $Pb(1,10\text{-phen})(S_2CNBu_2)_2$, (c,d) $Pb(S_2COBu)_2$, (e,f) $Pb(S_2COHex)_2$, and (g,h) $Pb(S_2COOct)_2$. Xanthate samples (c−h) shown with low (left column) and high magnifigcation images (right column) to illustrate both the film homogeneity and detail of the PbS nanostructures.

in the initial burst. This mechanism is consistent with the TGA data (Supporting Information Figure 1); the dithiocarbamate complexes show higher decomposition temperatures than the xanthate complexes, meaning the extent of nucleation is less, so fewer nuclei are formed initially and, consequently, larger particles grow. The lower decomposition temperatures of the three xanthate complexes result in a rapid nucleation burst, leading to films containing a large number of smaller, homogeneously distributed nanocrystals, as required for photovoltaic applications.

Changing the length of the xanthate chain lead to distinct morphological differences in films produced under otherwise identical conditions. The $Pb(S_2COBu)_2$ and $Pb(S_2COHex)_2$ samples give films containing PbS nanocubes which form dense interconnected networks. The cubes in the $Pb(S_2COBu)_2$ sample are noticeably larger than those for $Pb(S_2COHex)_2$, and TEM analysis revealed average widths of 104 ± 18 nm and 55 ± 12 nm for the butyl- and hexyl-xanthate complexes (Figure 5). In contrast, the $Pb(S_2COOct)_2$ sample appears to

DOI: 10.1021/cm504765z
Chem. Mater. 2015, 27, 2127−2136

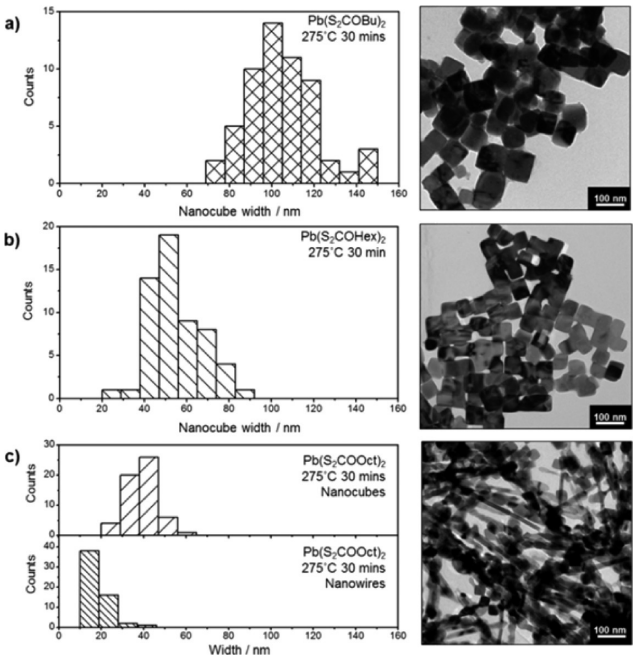

Figure 5. TEM size analysis of individual nanocrystals extracted from the PbS–polymer composite films. The size analysis of over 50 particles (left column) and a typical TEM image (right column) are shown for (a) $Pb(S_2COBu)_2$ (film shown in Figure 4c,d), (b) $Pb(S_2COHex)_2$ (film shown in Figure 4e,f), and (c) $Pb(S_2COOct)_2$ (film shown in Figure 4g,h).

contain a mixture of PbS nanowires (average width 18 ± 5 nm) and PbS nanocubes (average width 38 ± 7 nm nm). We have demonstrated size control through precursor choice. Use of precursors with increased xanthate chain length reduces the critical dimensions of the nanocrystals formed. Shape control is also possible with the $Pb(S_2COOct)_2$ precursor, which leads to anisotropic growth.

Recent work on the domain size control of CdS-P3HT films has, through choice of the cadmium(II) xanthate precursor used, shown control of polymer domain sizes depending on the solubility of the complex used.[33] However, this work suggests that the size of CdS crystals remains constant for all precursors used, but the extent of agglomeration of the CdS nanocrystals is reduced when using longer alkyl chain xanthate ligands.[33] In contrast our work clearly demonstrates that, for lead(II) xanthates, changing the length of the xanthate ligands effects both the size and shape of the PbS nanocrystals formed.

HRTEM analysis allows the crystallographic orientation of individual nanostrucutures to be determined (Figure 6). The nanocubes are all found to be single crystals, with the six faces of the cube corresponding to the {100} planes of PbS, which is consistent with previous reports of PbS nanocube synthesis.[43,58,59] The literature contains many examples of PbS nanowires with elongation in the [100],[60−64] [112],[60] [111],[65] or [011] direction,[60,66] depending upon the growth mechanism and reaction conditions. HRTEM analysis revealed that all the nanowires in the $Pb(S_2COOct)_2$ samples are elongated in the [011] direction, demonstrating that the formation of nanowires is not by growth from one of the (100) faces of a nanocube seed nor by face-on-face oriented attachment of nanocubes.[67] Also zigzag surfaces expected for [011] elongated PbS nanowires grown by oriented attachment of nanocubes were not observed.[65,68]

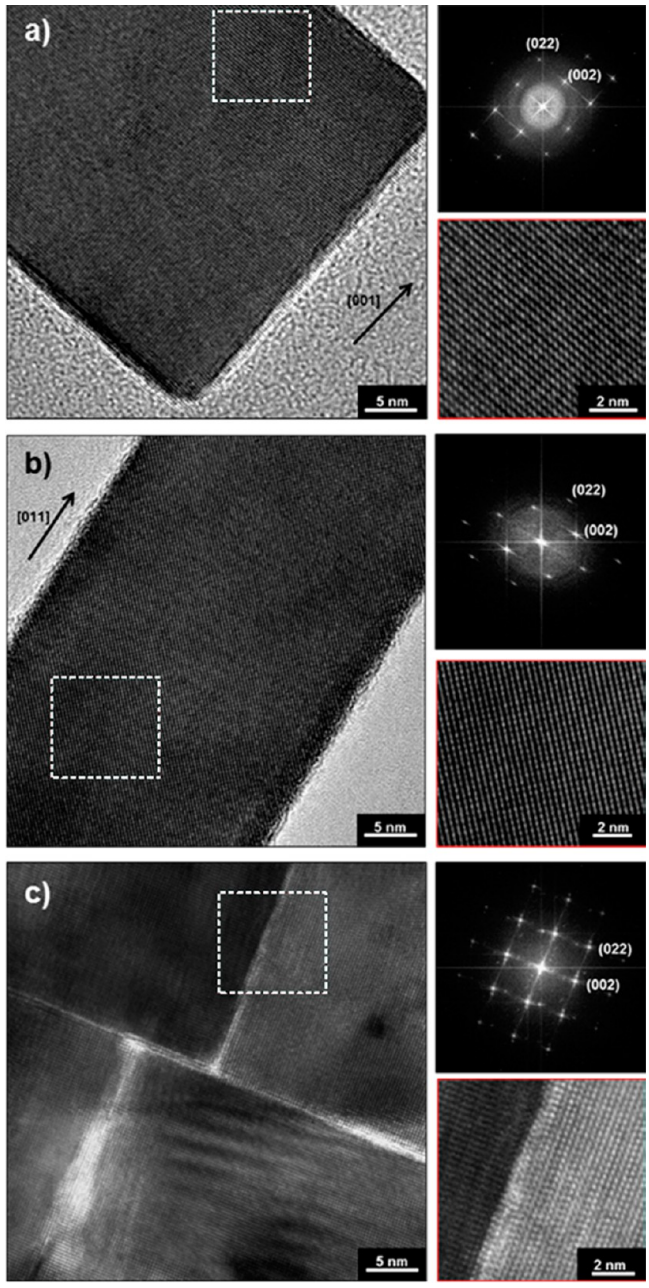

Figure 6. HRTEM images of PbS nanocrystals formed from (a) $Pb(S_2COBu)_2$, (b) $Pb(S_2COOct)_2$, and (c) $Pb(S_2COHex)_2$. The HRTEM images are accompanied by the Fourier transform (upper right of main image) and an enlarged area indicated by the dashed box (lower right of main image) to clearly show the lattice fringes and atomically intimate contact between nanocrystals.

TEM analysis of the $Pb(S_2COOct)_2$ films showed PbS nanowires connected to a nanocube (Supporting Information Figure 5). The nanowires emerge from the cubes in the [011] direction. These cube terminations suggest that the nanowires may grow from an edge site on a nanocube seed. The distinct morphology observed in the $Pb(S_2COOct)_2$ sample may be correlated to the TGA data (Supporting Information Figure 1). $Pb(S_2COOct)_2$ undergoes a two-step decomposition, which would be consistent with our postulated two-stage growth mechanism: with initial formation of nanocubes followed by the growth of nanowires from nanocube seeds. This mechanism

DOI: 10.1021/cm504765z
Chem. Mater. 2015, 27, 2127−2136

may explain the observation of nanocubes in all nanowire containing films.

3.4. Evidence of Ligand Free Interfaces. A major attraction of this method is the potential absence of capping ligands; better charge transfer at PbS−polymer interfaces and better charge percolation through nanocrystal networks should be observed. It has previously been shown that capping ligands lead to separation between adjacent particles in TEM images and measurement of this distance can be used to infer the nature of capping.[69−71]

The HRTEM images showed the nanocubes from the $Pb(S_2COBu)_2$ and $Pb(S_2COHex)_2$ precursors to have {100} faces (Figure 6a,c), while the nanowires grown form the $Pb(S_2COOct)_2$ precursor are shown to grow in the [011] direction. In the HRTEM images, aggregated nanocrystals were observed with no separation from their neighbors (Figure 6c). Such images suggest atomically intimate interfaces and provide evidence supporting ligand free surfaces.

3.5. Effect of Heating Conditions on the Extent of Precursor Conversion. XRD analysis of films prepared using temperatures from 80 to 275 °C shows that the extent of precursor decomposition is temperature dependent (Figure 7). Lower temperatures are attractive for flexible solar cell application,[30,50] but too low a temperature can result in only partial decomposition of the precursor. Figure 7 shows that $Pb(S_2COBu)_2$ gives a mixture of PbS and precursor at 80 or 100 °C. Complete decomposition is seen when the films are heated for 30 min at 150 °C or higher. A similar trend is seen in all three of the xanthates investigated: 100 °C for 30 min gives incomplete decomposition but 150 °C (30 min) results in complete conversion to PbS (Supporting Information Figure 6).

The amount of undecomposed precursor present at a particular temperature can be reduced by increasing the heating time. XRD patterns for $Pb(S_2COBu)_2$−polymer films heated at 100 °C for various times from 30 to 120 min (Supporting Information Figure 7) show that as the time is increased the intensity of peaks corresponding to unreacted precursor reduce. However, 120 min is required for complete decomposition at 100 °C, compared to 30 min at 150 °C.

3.6. Effect of Temperature on Film Morphology. The XRD patterns in Figure 7 show that the temperature also affects the film structure. The film prepared by heating at 275 °C gave intense (200) and (400) peaks, indicating [100] orientation. In contrast, at lower temperatures the relative peaks intensities suggest more randomly oriented nanocrystals.[72] SEM BSE images of $Pb(S_2COBu)_2$ films prepared at different heating temperatures are shown in Figure 8. All contained interconnected networks of PbS nanocubes. The films prepared at 275 °C contain significantly larger particles than those from lower temperatures, with TEM (Supporting Information Figure 8) showing average widths of 46 ± 14 nm and 104 ± 18 nm for 100 and 275 °C (both 30 min). This result is interesting as one

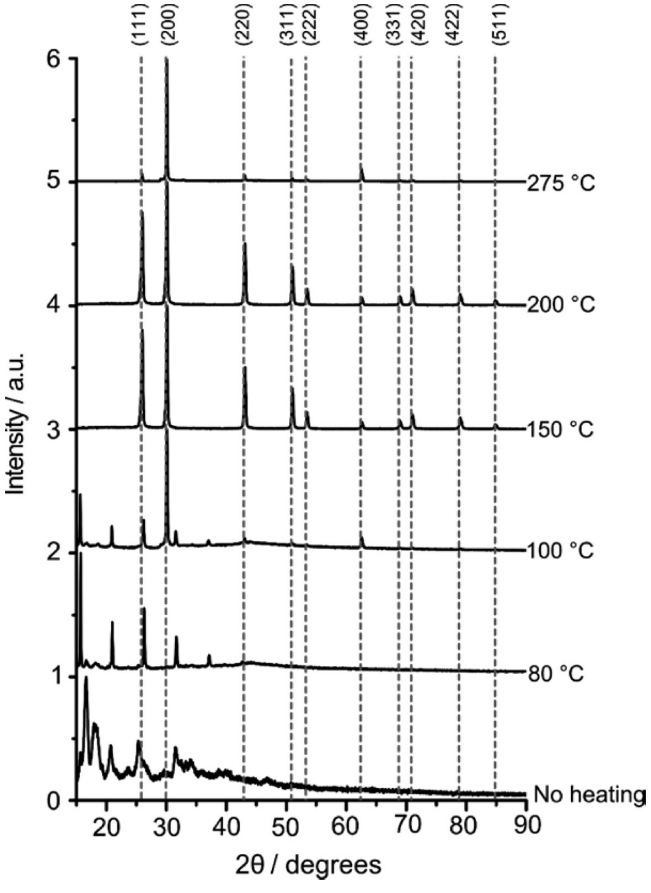

Figure 7. XRD patterns for films from $Pb(S_2COBu)_2$. All films were heated for 30 min at the temperatures shown. Peaks corresponding to the unreacted precursor are not present after heating above 150 °C. The reference peak positions for PbS galena 00-005-0592 are shown with dashed lines.

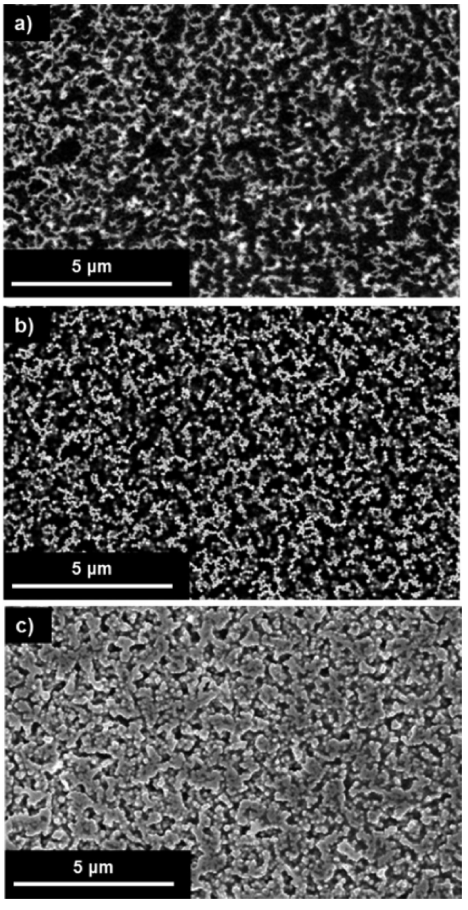

Figure 8. Backscattered SEM images of films made with $Pb(S_2COBu)_2$ precursor. All films were heated for 30 min at (a) 100 °C, (b) 200 °C, and (c) 275 °C.

DOI: 10.1021/cm504765z
Chem. Mater. 2015, 27, 2127−2136

might expect faster supersaturation, more nuclei, and consequently smaller particles at the higher temperature. It seems possible that a nonclassical growth mechanism involving the coalescence of smaller nanocrystals to form large nanocubes occurs at the higher temperature. Heating PbS nanocrystal films at 200 °C has been previously shown to induce coalescence.[73]

Films prepared at 200 and 275 °C (Figure 8b,c) both contain the same loading of PbS, but the coverage of PbS nanocubes observed in the SEM images appears far higher in the 275 °C sample. However, SEM only probes the film surface; the more oriented material in the higher temperature films may lead to its apparently higher coverage. During the high temperature processing a transformation from a three-dimensional to more two-dimensional distribution of PbS nanocubes may occur, with rafts of densely packed, oriented, PbS nanocubes forming near the surface of the film.

3.7. Low Temperature Processing. There is considerable interest in fabricating hybrid films on plastic substrates to create flexible photovoltaics,[17] for compatibility with suitable substrates low processing temperatures, typically less than 160 °C, are required.[30] $Pb(S_2COBu)_2$, $Pb(S_2COHex)_2$, and $Pb(S_2COOct)_2$ all show complete conversion to PbS at 150 °C, demonstrating the potential for long chain xanthate complexes to form high quality PbS−polymer hybrid films at low temperatures.

Figure 9 shows the morphologies of films produced by heating the three xanthate precursors at 150 °C for 30 min. Accompanying XRD patterns can be found in Figure 7 and Supporting Information Figure 6. As with the higher temperature films (Figure 4), the choice of precursor influences film morphology. The films from butyl- and hexyl-xanthate complexes contain nanocubes, with $Pb(S_2COHex)_2$ forming smaller cubes. The $Pb(S_2COOct)_2$ forms a mixture of PbS nanowires and smaller nanocubes; however, nanowires are less prevalent than in the 275 °C sample. The XRD of the $Pb(S_2COHex)_2$ sample heated at 150 °C shows the same [100] orientation and high apparent coverage seen for the $Pb(S_2COBu)_2$ derived films grown at 275 °C. We attribute these features to the formation of two-dimensional rafts of nanocubes, a theory supported by the SEM images in Figure 9b. This orientation is not seen in material grown from $Pb(S_2COBu)_2$ at 150 °C. The results clearly demonstrate that the morphology of the films can be controlled by precursor choice and temperature, even while employing low processing temperatures.

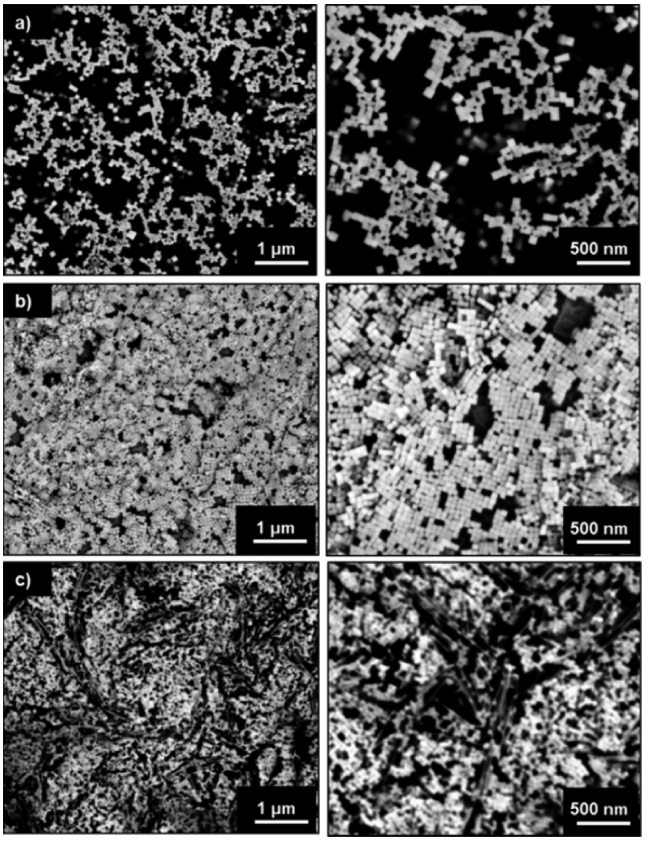

Figure 9. Backscattered SEM images of films made at low heating temperatures. Films made by heating precursor−polymer films at 150 °C for 30 min with (a) $Pb(S_2COBu)_2$, (b) $Pb(S_2COHex)_2$, and (c) $Pb(S_2COOct)_2$. XRD shows that in all films the precursor has been fully converted to PbS (Figure 7 and Supporting Information Figure 6).

4. CONCLUSIONS

This work demonstrates the first successful synthesis of PbS−polymer hybrid materials by decomposition of molecular precursors in polymer films. We have investigated a range of single source precursors. The lower decomposition temperatures of lead(II) xanthate complexes may make them preferable to the dithiocarbamate complexes. The xanthate complexes allow the low temperature synthesis of continuous, adherent films of homogeneous composition containing PbS nanostructures of a narrow size and defined shape. Nanodimensional domains of PbS and polymer phases along with the highly interconnected networks of PbS nanocrystals seen in these films are potentially attractive architectures for solar cell applications, particularly when combined with the evidence of potentially ligand-free interfaces between adjacent nanocrystals. The longer chain xanthates ($Pb(S_2COBu)_2$, $Pb(S_2COHex)_2$, and $Pb(S_2COOct)_2$) have good solubility in organic solvents and decompose cleanly to give pure PbS−polymer films under favorable processing conditions (30 min at 150 °C). These properties make these precursors potentially compatible with roll-to-roll processing and flexible plastic substrates. We have demonstrated that morphological control is possible though precursor chemistry: increasing xanthate chain length leads to reduced nanocrystal dimensions. The precursor structure or its mechanism or temperature of decomposition influence nanocrystal shape. $Pb(S_2COBu)_2$ and $Pb(S_2COHex)_2$ form PbS nanocubes but $Pb(S_2COOct)_2$ gives PbS nanowires. This may allow simple, scalable fabrication and ligand-free interfaces to be combined with both size and shape control. Further investigations are planned to apply this control to the in situ fabrication of PbS−polymer photovoltaic devices.

■ ASSOCIATED CONTENT

Supporting Information

Additional TGA curves, XRD data, TEM images, and crystallographic information. This material is available free of charge via the Internet at http://pubs.acs.org.

■ AUTHOR INFORMATION

Corresponding Authors

*(S.J.H.) E-mail: sarah.haigh@manchester.ac.uk.
*(P.O.B.) E-mail: paul.o'brien@manchester.ac.uk.

DOI: 10.1021/cm504765z
Chem. Mater. 2015, 27, 2127−2136

Author Contributions

The manuscript was written through contributions of all authors.

Notes

The authors declare no competing financial interest.

■ ACKNOWLEDGMENTS

S.J.H. and E.A.L. acknowledge funding from multiple research grants including the Engineering and Physical Sciences Research Council (EPSRC) UK Grants EP/G035954/1 and EP/J021172/1 and Defence Threat Reduction Agency Grant HDTRA1-12-1-0013. E.A.L. would like to thank the North West Nanoscience Doctoral Training Centre (NOWNano DTC) for supporting his work. The FEI Magellan SEM is part of University of Manchester LATEST2 programme, funded by EPSRC Grant EP/H020047/1. P.O.B. and P.D.M. acknowledge funding from EPSRC UK Grants EP/K010298/1 and EP/K039547/1. The authors would like to thank the Royal Society (London) Leverhulme Africa Award Program for funding S.A.S.'s study at the University of Manchester.

■ REFERENCES

(1) Oosterhout, S. D.; Wienk, M. M.; van Bavel, S. S.; Thiedmann, R.; Koster, L. J. A.; Gilot, J.; Loos, J.; Schmidt, V.; Janssen, R. A. J. *Nat. Mater.* **2009**, *8*, 818.
(2) Seo, J.; Cho, M. J.; Lee, D.; Cartwright, A. N.; Prasad, P. N. *Adv. Mater.* **2011**, *23*, 3984.
(3) Huynh, W. U.; Dittmer, J. J.; Alivisatos, A. P. *Science* **2002**, *295*, 2425.
(4) Dowland, S.; Lutz, T.; Ward, A.; King, S. P.; Sudlow, A.; Hill, M. S.; Molloy, K. C.; Haque, S. A. *Adv. Mater.* **2011**, *23*, 2739.
(5) Leventis, H. C.; King, S. P.; Sudlow, A.; Hill, M. S.; Molloy, K. C.; Haque, S. A. *Nano Lett.* **2010**, *10*, 1253.
(6) Coe-Sullivan, S.; Woo, W.-K.; Steckel, J. S.; Bawendi, M.; Bulović, V. *Org. Electron.* **2003**, *4*, 123.
(7) Borriello, C.; Masala, S.; Bizzarro, V.; Nenna, G.; Re, M.; Pesce, E.; Minarini, C.; Di Luccio, T. *J. Appl. Polym. Sci.* **2011**, *122*, 3624.
(8) Colvin, V. L.; Schlamp, M. C.; Alivisatos, A. P. *Nature* **1994**, *370*, 354.
(9) Anikeeva, P. O.; Halpert, J. E.; Bawendi, M. G.; Bulović, V. *Nano Lett.* **2009**, *9*, 2532.
(10) Rauch, T.; Boberl, M.; Tedde, S. F.; Furst, J.; Kovalenko, M. V.; Hesser, G.; Lemmer, U.; Heiss, W.; Hayden, O. *Nat. Photonics* **2009**, *3*, 332.
(11) Yuan, C.; Xu, Y.; Deng, Y.; Jiang, N.; He, N.; Lizong, D. *Nanotechnology* **2010**, *21*, 415501.
(12) Peng, H.; Soeller, C.; Cannell, M. B.; Bowmaker, G. A.; Cooney, R. P.; Travas-Sejdic, J. *Biosens. Bioelectron.* **2006**, *21*, 1727.
(13) Gao, F.; Ren, S.; Wang, J. *Energy Environ. Sci.* **2013**, *6*, 2020.
(14) Moule, A. J.; Chang, L.; Thambidurai, C.; Vidu, R.; Stroeve, P. *J. Mater. Chem.* **2012**, *22*, 2351.
(15) Zhou, R.; Xue, J. *ChemPhysChem* **2012**, *13*, 2471.
(16) Krebs, F. C.; Gevorgyan, S. A.; Alstrup, J. *J. Mater. Chem.* **2009**, *19*, 5442.
(17) Pagliaro, M.; Ciriminna, R.; Palmisano, G. *ChemSusChem* **2008**, *1*, 880.
(18) Jangwon, S.; Sung Jin, K.; Won Jin, K.; Rohit, S.; Marek, S.; Alexander, N. C.; Paras, N. P. *Nanotechnology* **2009**, *20*, 095202.
(19) Leventis, H. C.; O'Mahony, F.; Akhtar, J.; Afzaal, M.; O'Brien, P.; Haque, S. A. *J. Am. Chem. Soc.* **2010**, *132*, 2743.
(20) Semonin, O. E.; Luther, J. M.; Choi, S.; Chen, H.-Y.; Gao, J.; Nozik, A. J.; Beard, M. C. *Science* **2011**, *334*, 1530.
(21) Hardman, S. J. O.; Graham, D. M.; Stubbs, S. K.; Spencer, B. F.; Seddon, E. A.; Fung, H.-T.; Gardonio, S.; Sirotti, F.; Silly, M. G.; Akhtar, J.; O'Brien, P.; Binks, D. J.; Flavell, W. R. *Phys. Chem. Chem. Phys.* **2011**, *13*, 20275.
(22) Sambur, J. B.; Novet, T.; Parkinson, B. A. *Science* **2010**, *330*, 63.
(23) McDonald, S. A.; Konstantatos, G.; Zhang, S. G.; Cyr, P. W.; Klem, E. J. D.; Levina, L.; Sargent, E. H. *Nat. Mater.* **2005**, *4*, 138.
(24) McDonald, S. A.; Cyr, P. W.; Levina, L.; Sargent, E. H. *Appl. Phys. Lett.* **2004**, *85*, 2089.
(25) Martínez-Ferrero, E.; Albero, J.; Palomares, E. *J. Phys. Chem. Lett.* **2010**, *1*, 3039.
(26) Greenham, N. C.; Peng, X.; Alivisatos, A. P. *Phys. Rev. B* **1996**, *54*, 17628.
(27) von Holt, B.; Kudera, S.; Weiss, A.; Schrader, T. E.; Manna, L.; Parak, W. J.; Braun, M. *J. Mater. Chem.* **2008**, *18*, 2728.
(28) Rath, T.; Trimmel, G. *Hybrid Mater.* **2014**, *1*, 15.
(29) Rath, T.; Edler, M.; Haas, W.; Fischereder, A.; Moscher, S.; Schenk, A.; Trattnig, R.; Sezen, M.; Mauthner, G.; Pein, A.; Meischler, D.; Bartl, K.; Saf, R.; Bansal, N.; Haque, S. A.; Hofer, F.; List, E. J. W.; Trimmel, G. *Adv. Energy Mater.* **2011**, *1*, 1046.
(30) Fradler, C.; Rath, T.; Dunst, S.; Letofsky-Papst, I.; Saf, R.; Kunert, B.; Hofer, F.; Resel, R.; Trimmel, G. *Sol. Energy Mater. Sol. C* **2014**, *124*, 117.
(31) Bansal, N.; O'Mahony, F. T. F.; Lutz, T.; Haque, S. A. *Adv. Energy Mater.* **2013**, *3*, 986.
(32) Reynolds, L. X.; Lutz, T.; Dowland, S.; MacLachlan, A.; King, S.; Haque, S. A. *Nanoscale* **2012**, *4*, 1561.
(33) MacLachlan, A. J.; Rath, T.; Cappel, U. B.; Dowland, S. A.; Amenitsch, H.; Knall, A.-C.; Buchmaier, C.; Trimmel, G.; Nelson, J.; Haque, S. A. *Adv. Funct. Mater.* **2015**, *25*, 409.
(34) Antolini, F.; Di Luccio, T.; Laera, A. M.; Mirenghi, L.; Piscopiello, E.; Re, M.; Tapfer, L. *Phys. Status Solidi B* **2007**, *244*, 2768.
(35) Athanassiou, A.; Blasi, L.; De Giorgi, M.; Caputo, G.; Fragouli, D.; Tsiranidou, E.; Laera, A. M.; Tapfer, L.; Cingolani, R. *Polym. Compos.* **2010**, *31*, 1075.
(36) Kaltenhauser, V.; Rath, T.; Haas, W.; Torvisco, A.; Muller, S. K.; Friedel, B.; Kunert, B.; Saf, R.; Hofer, F.; Trimmel, G. *J. Mater. Chem. C* **2013**, *1*, 7825.
(37) Malik, M. A.; Afzaal, M.; O'Brien, P. *Chem. Rev.* **2010**, *110*, 4417.
(38) Fan, D.; Afzaal, M.; Mallik, M. A.; Nguyen, C. Q.; O'Brien, P.; Thomas, P. J. *Coord. Chem. Rev.* **2007**, *251*, 1878.
(39) Pickett, N. L.; O'Brien, P. *Chem. Rec.* **2001**, *1*, 467.
(40) Lewis, E.; Haigh, S.; O'Brien, P. *J. Mater. Chem. A* **2014**, *2* (3), 570−580.
(41) Lazell, M.; O'Brien, P.; Otway, D. J.; Park, J.-H. *Dalton Trans.* **2000**, 4479.
(42) Cant, D. J. H.; Syres, K. L.; Lunt, P. J. B.; Radtke, H.; Treacy, J.; Thomas, P. J.; Lewis, E. A.; Haigh, S. J.; O'Brien, P.; Schulte, K.; Bondino, F.; Magnano, E.; Flavell, W. R. *Langmuir* **2015**, *31*, 1445.
(43) Zhou, G. J.; Lu, M. K.; Xiu, Z. L.; Wang, S. F.; Zhang, H. P.; Zhou, Y. Y.; Wang, S. M. *J. Phys. Chem. B* **2006**, *110*, 6543.
(44) Lee, S. M.; Cho, S. N.; Cheon, J. *Adv. Mater.* **2003**, *15*, 441.
(45) Thanh, N. T. K.; Maclean, N.; Mahiddine, S. *Chem. Rev.* **2014**, *114* (15), 7610.
(46) Hindson, J. C.; Saghi, Z.; Hernandez-Garrido, J.-C.; Midgley, P. A.; Greenham, N. C. *Nano Lett.* **2011**, *11*, 904.
(47) Gur, I.; Fromer, N. A.; Chen, C.-P.; Kanaras, A. G.; Alivisatos, A. P. *Nano Lett.* **2006**, *7*, 409.
(48) Bansal, A. K.; Antolini, F.; Sajjad, M. T.; Stroea, L.; Mazzaro, R.; Ramkumar, S. G.; Kass, K. J.; Allard, S.; Scherf, U.; Samuel, I. D. W. *Phys. Chem. Chem. Phys.* **2014**, *16*, 9556.
(49) Afzaal, M.; Ellwood, K.; Pickett, N. L.; O'Brien, P.; Raftery, J.; Waters, J. *J. Mater. Chem.* **2004**, *14*, 1310.
(50) Akhtar, J.; Afzaal, M.; Vincent, M. A.; Burton, N. A.; Hillier, I. H.; O'Brien, P. *Chem. Commun.* **2011**, *47*, 1991.
(51) Akhtar, J.; Malik, M. A.; O'Brien, P.; Wijayantha, K. G. U.; Dharmadasa, R.; Hardman, S. J. O.; Graham, D. M.; Spencer, B. F.; Stubbs, S. K.; Flavell, W. R.; Binks, D. J.; Sirotti, F.; El Kazzi, M.; Silly, M. *J. Mater. Chem.* **2010**, 20.
(52) Akhtar, J.; Malik, M. A.; O'Brien, P.; Helliwell, M. *J. Mater. Chem.* **2010**, *20*, 6116.

DOI: 10.1021/cm504765z
Chem. Mater. 2015, 27, 2127−2136

(53) Pradhan, N.; Katz, B.; Efrima, S. *J. Phys. Chem. B* **2003**, *107*, 13843.
(54) Wright, M.; Uddin, A. *Sol. Energy Mater. Sol. C* **2012**, *107*, 87.
(55) Jung, Y. K.; Kim, J. I.; Lee, J.-K. *J. Am. Chem. Soc.* **2010**, *132* (1), 178−184.
(56) Zubkowski, J. D.; Hall, T.; Valente, E. J.; Perry, D. L.; Feliu, L. A.; Garmon, J. *J. Chem. Crystallogr.* **1997**, *27*, 251.
(57) Jiang, C.; Liu, W.; Talapin, D. V. *Chem. Mater.* **2014**, *26*, 4038.
(58) Lihong, D.; Ying, C.; Yujiang, Z.; Wei, Z. *Nanotechnology* **2009**, *20*, 125301.
(59) Quan, Z. W.; Li, C. X.; Zhang, X. M.; Yang, J.; Yang, P. P.; Zhang, C. M.; Lin, J. *Cryst. Growth Des.* **2008**, *8*, 2384.
(60) Jang, S. Y.; Song, Y. M.; Kim, H. S.; Cho, Y. J.; Seo, Y. S.; Jung, G. B.; Lee, C.-W.; Park, J.; Jung, M.; Kim, J.; Kim, B.; Kim, J.-G.; Kim, Y.-J. *ACS Nano* **2010**, *4*, 2391.
(61) Yu, D.; Wang, D.; Meng, Z.; Lu, J.; Qian, Y. *J. Mater. Chem.* **2002**, *12*, 403.
(62) Bierman, M. J.; Lau, Y. K. A.; Jin, S. *Nano Lett.* **2007**, *7*, 2907.
(63) Sun, J.; Buhro, W. E. *Angew. Chem., Int. Ed.* **2008**, *120*, 3259.
(64) Afzaal, M.; O'Brien, P. *J. Mater. Chem.* **2006**, *16*, 1113.
(65) Akhtar, J.; Malik, M. A.; O'Brien, P.; Revaprasadu, N. *Mater. Lett.* **2012**, *77*, 78.
(66) Warner, J. H.; Cao, H. *Nanotechnology* **2008**, *19*, 305605.
(67) Talapin, D. V.; Yu, H.; Shevchenko, E. V.; Lobo, A.; Murray, C. B. *J. Phys. Chem. C* **2007**, *111*, 14049.
(68) Cho, K. S.; Talapin, D. V.; Gaschler, W.; Murray, C. B. *J. Am. Chem. Soc.* **2005**, *127*, 7140.
(69) Huo, Z.; Chen, C.; Li, Y. *Chem. Commun.* **2006**, 3522.
(70) Dumestre, F.; Chaudret, B.; Amiens, C.; Renaud, P.; Fejes, P. *Science* **2004**, *303*, 821.
(71) Sivaraman, S. K.; Santhanam, V. *Nanotechnology* **2012**, *23*, 255603.
(72) Kanniainen, T.; Lindroos, S.; Ihanus, J.; Leskela, M. *J. Mater. Chem.* **1996**, *6*, 161.
(73) Jo, C. H.; Kim, J. H.; Kim, J.; Kim, J.; Oh, M. S.; Kang, M. S.; Kim, M.-G.; Kim, Y.-H.; Ju, B.-K.; Park, S. K. *J. Mater. Chem. C* **2014**, *2*, 10305.

DOI: 10.1021/cm504765z
Chem. Mater. 2015, 27, 2127−2136